physica status solidi b
www.pss-b.com

Check for updates

# Two-Dimensional Wetting Layer Structures of Reduced Ternary Oxides on Ru(0001) and Pt(111)

*Eva Maria Zollner, Fabian Schuster, Klaus Meinel, Philine Stötzner, Sebastian Schenk, Bettina Allner, Stefan Förster,* and Wolf Widdra*

**Long-range ordered structures of reduced oxide films with monolayer thickness derived from $BaTiO_3$ and $SrTiO_3$ on Ru(0001) and Pt(111) are investigated by scanning tunneling microscopy (STM) and low-energy electron diffraction (LEED). Upon ultrahigh vacuum annealing at 1100 K, a hexagonal phase is observed for $BaTiO_3$ on Ru(0001), which forms similarly from $SrTiO_3$ on Pt(111). At higher temperatures, a triangle–square tiling called σ-phase develops in the $BaTiO_3$/Ru(0001) system, with a unit cell rotation of 15° against the Ru(0001) substrate. Furthermore, it is shown that this 15° rotated σ-phase also forms in the $BaTiO_3$/Pt(111) system in addition to the already known 8° rotated σ-phase. The results emphasize a strong flexibility in the structural parameters of the reduced oxide wetting layers in response to the substrate interaction strength.**

## 1. Introduction

The discovery of a 2D quasicrystalline structure derived from $BaTiO_3$ on the Pt(111) surface opened a new chapter in the heteroepitaxy at interfaces.[1] This system is the first example for a spontaneous formation of a dodecagonal symmetry on a sixfold substrate on the atomic level.

The opposite, the formation of periodic structures on quasicrystal surfaces, is known from the beginning of quasicrystal research: periodic overlayers emerged at the surfaces of bulk-quasicrystals upon slightly altering the sample composition at the surface.[2–4] They have also been formed in many investigations of solid films deposited on quasicrystal surfaces.[5–7]

The epitaxial alignment of an overlayer to the substrates has many ingredients. It results from an interplay of interactions within the overlayer and between the overlayer and the substrate. They are linked to the chemical nature of the constituents, the symmetry, or the misfit between the two systems and can induce significant strain in the overlayer.[8] Different types of crystal–crystal epitaxy are classified according to their superstructure matrix coefficients. Integer coefficients report on a commensurate alignment, fractional coefficients describe higher-order-commensurate structures, and irrational coefficients are the signature of incommensurate structures. Additional types can be distinguished in reciprocal space, e.g., the point-on-line symmetry for which substrate and superstructure spots coincide along a line.[9] The basics theory to describe epitaxy in periodic systems is the coincidence-site-lattice (CSL) theory.[10–12] This theory has been expanded to interfaces of periodic structures with quasicrystals in the formulation of the coincidence reciprocal lattice planes (CRLP) theory.[13] The observation of a coincidence of reciprocal lattice points of a periodic overlayer on a bulk quasicrystal is an even stronger criterion for stabilizing an epitaxial quasicrystal–crystal interface.[14]

The peculiar long-range order of oxide quasicrystals (OQCs) develops in a wetting layer of reduced $BaTiO_3$ or $SrTiO_3$ that forms upon annealing in ultrahigh vacuum on the Pt(111) surface.[1,15–17] A comprehensive introduction into different aspects ranging from a statistical tiling analysis to electronic properties is given by Förster et al. in this issue.[18] For higher preparation temperatures, a transition of the wetting layer toward a periodic approximant structure is observed for $BaTiO_3$/Pt(111).[19] This approximant forms a σ-phase tiling with four triangles and two squares in the unit cell. It is described by a $\begin{pmatrix} 27/5 & 2 \\ 3/4 & 5 \end{pmatrix}$ superstructure matrix corresponding to a 8° rotation.[19–21] Its higher-order commensurate cell described by $\begin{pmatrix} 27 & 10 \\ 3 & 20 \end{pmatrix}$ contains a patch of $4 \times 5$ primitive unit cells. In the closely related system of $SrTiO_3$/Pt(111), small patches of the OQC develop embedded in extended domains of a larger unit cell approximant.[15] This approximant contains 36 tiles of the OQC in its unit cell and forms a commensurate lattice described by a $\begin{pmatrix} 9 & 0 \\ 16 & 9 \end{pmatrix}$ matrix.

E. Maria Zollner, F. Schuster, Dr. K. Meinel, P. Stötzner, S. Schenk, B. Allner, Dr. S. Förster, Prof. W. Widdra
Institute of Physics
Martin-Luther-Universität Halle-Wittenberg
D-06099 Halle, Germany
E-mail: stefan.foerster@physik.uni-halle.de

Prof. W. Widdra
Max-Planck-Institut für Mikrostrukturphysik
D-06120 Halle, Germany

The ORCID identification number(s) for the author(s) of this article can be found under https://doi.org/10.1002/pssb.201900655.

© 2020 The Authors. Published by WILEY-VCH Verlag GmbH & Co. KGaA, Weinheim. This is an open access article under the terms of the Creative Commons Attribution-NonCommercial License, which permits use, distribution and reproduction in any medium, provided the original work is properly cited and is not used for commercial purposes.

**DOI: 10.1002/pssb.201900655**

Here, we report on 2D wetting layer structures formed from $BaTiO_3$ on Ru(0001), which we also found in $SrTiO_3$/Pt(111) and $BaTiO_3$/Pt(111). Upon annealing an initially 0.4 nm thin $BaTiO_3$ layer on Ru(0001) to 1100 K, we observe the formation of a long-range ordered wetting layer structure. Its nature is different as compared with the aforementioned OQC and its approximants, as the interatomic distance of the Ti ions in the layer is a factor of two smaller. This structure also forms in slightly Ti-enriched layers of $SrTiO_3$ on Pt(111). Upon annealing $BaTiO_3$ on Ru(0001) at 1250 K, this structure is transformed into the $\sigma$-phase. The latter forms a commensurate lattice on Ru(0001) and is rotated by 15° against the Ru(0001) substrate. As reported here, this orientation can also occur for $BaTiO_3$/Pt(111), in addition to the already known 8° rotation of the $\sigma$-phase in this system.[19]

## 2. Results

For fabricating 2D layers of $BaTiO_3$ on Ru(0001), 0.4 nm of $BaTiO_3$ have been deposited by molecular beam epitaxy (MBE) at room temperature (RT). The as-deposited $BaTiO_3$ has been fully oxidized by annealing to 900 K in $10^{-5}$ mbar $O_2$. Upon subsequent annealing in ultrahigh vacuum (UHV) at 1100 K, a long-range ordered superstructure is formed. In large-scale scanning tunneling microscopy (STM) images, the surface exhibits extended terraces separated by monoatomic steps. On smaller scale, a superstructure is observed that entirely covers the Ru(0001) terraces. **Figure 1**a shows this structure in atomic resolution on a scale of $25 \times 12.5\,nm^2$. Up to four atoms are grouped together at the surface. On the first glance, their arrangement seems random. However, the Fourier transform (FT) of the image shown as inset in Figure 1a reveals a long-range hexagonal order. In the close-up image in Figure 1b, the hexagonal unit cell is shown. It consists of individual atoms that are the center atoms of a windmill-like building block. Six rhombs of four atoms are arranged around these centers. This structure arises as shown in Figure 1c from a small-scale hexagonal lattice. By displacing the atoms to groups of four around a central atom, a $\begin{pmatrix} 4 & 1 \\ 3 & 4 \end{pmatrix}$ superstructure is created. According to the matrix, the superstructure lattice is enlarged by a factor of $\sqrt{13} \times (\approx 3.6)$ and rotated by 12.1°. In the FT of the STM image of Figure 1a, both lattices can be recognized. In addition to the superstructure lattice marked by the red circles, the primitive hexagonal mesh gives rise to the high intensities of the outer spots marked by the blue circles.

This structure exhibits a chirality with respect to the arrangement of rhombs. In Figure 1b,c, a windmill with clockwise rotation is indicated. In addition, windmills with a counter clockwise rotation have been found on other terraces (not shown here). However, the rotation remains constant on one terrace and there are no phase boundaries on a terrace. From previous STM studies for 2D superstructures of reduced $BaTiO_3$ on Pt(111), it is known that the Ti sublattice of the ternary oxide is seen in STM for bias voltages close the Fermi level.[1,19,22] These tunneling conditions apply here as well. Thus the contrast in STM is attributed to Ti atoms.

The low-energy electron diffraction (LEED) pattern of the structure is shown in Figure 1d. It reveals a flower-like diffraction

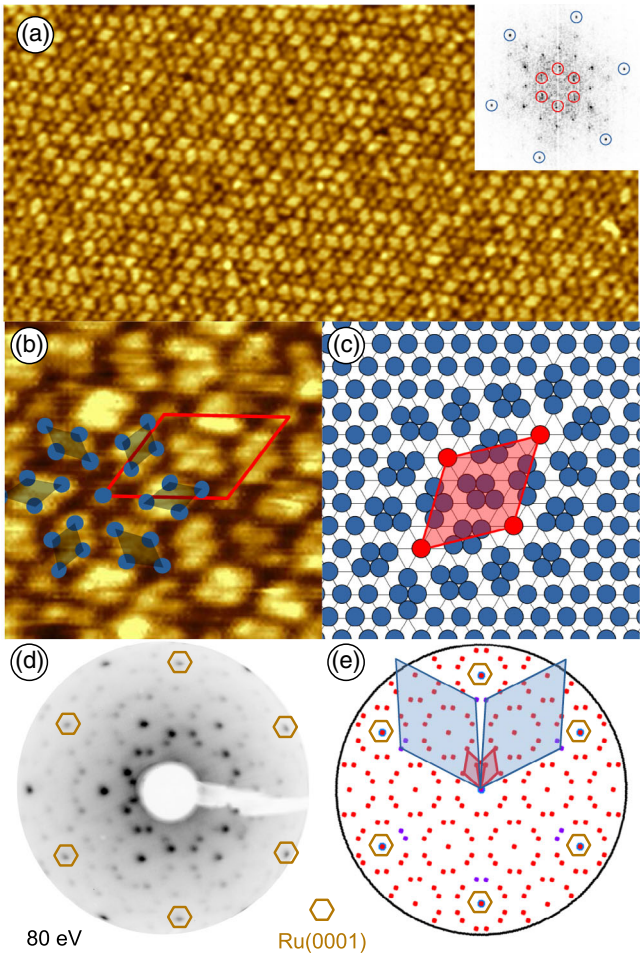


**Figure 1.** Hexagonal superstructure in a 2D network derived from $BaTiO_3$ on Ru(0001). The STM images (a,b) reveal a windmill-like pattern on the atomic scale. The hexagonal order is seen in the FT of the image (inset in (a)). The superstructure arises from systematic displacements of the atoms from a primitive hexagonal lattice as shown in (c). The d) measured and e) calculated LEED patterns show the formation of two rotational domains of a commensurate $\begin{pmatrix} 5 & 1 \\ 4 & 5 \end{pmatrix}$ superstructure. The unit cell of the windmill-like structure is marked red in (b,c,e), that of the primitive hexagonal cell of the overlayer is marked in blue. a) $25 \times 12.5\,nm^2$, b) $3.2 \times 3.2\,nm^2$, a,b) 170 pA, 1.1 V.

pattern that consists of groups of 12 equidistant spots around the substrate lattice spots and the respective $(\sqrt{3} \times \sqrt{3})R30°$ positions. In contrast to the fast Fourier transform (FFT) of the STM image, the LEED pattern represents a superposition of all rotational superstructure domains. A simulation of the LEED pattern determines a $\begin{pmatrix} 5 & 1 \\ 4 & 5 \end{pmatrix}$ superstructure in the reduced oxide layer with respect to Ru(0001). This corresponds to a lattice vector of 1.24 nm. The simulated LEED pattern is shown in Figure 1e. Two rotational domains of the superstructure exist at ±10.6° with respect to Ru(0001). These two domains give rise to the circles of 12 spots. In addition to the superstructure unit cell marked in red, the unit cell of the primitive hexagonal structure is marked in blue in the simulated pattern. In this


© 2020 The Authors. Published by WILEY-VCH Verlag GmbH & Co. KGaA, Weinheim

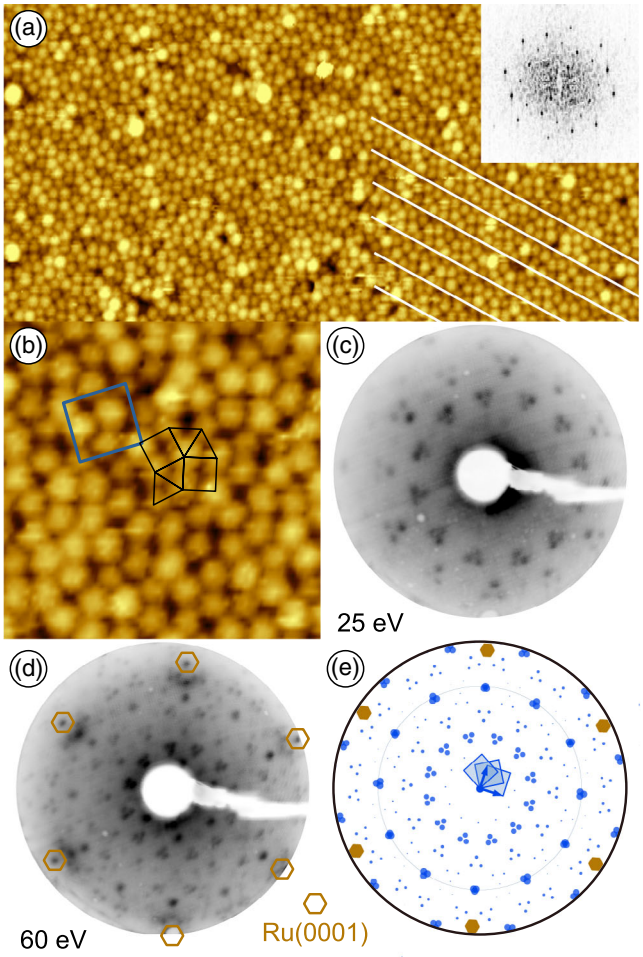


**Figure 2.** a,b) STM data of the $\sigma$-phase derived from $BaTiO_3$ on Ru(0001). The FT of (a) shown as an inset emphasizes a quadratic unit cell. The close-up image (b) reveals a triangle-square tiling. The unit cell is marked in blue and the characteristic motif of four triangles and two squares in black. c,d) The measured LEED pattern is characterized by triangular groups of spots every 30° at various reciprocal lengths. e) The simulated pattern was calculated using a $\begin{pmatrix} 4 & -1.5 \\ 4 & 5.5 \end{pmatrix}$ superstructure matrix. The pattern results from three domains as indicated in (e). The circle at 2.0 $Å^{-1}$ in (e) marks a diffraction order with systematic deviations from 12-fold symmetry. a) 19.3 × 9.7 $nm^2$, b) 6.6 × 6.6 $nm^2$, a,b) 130 pA, –2.6 V.

smallest scale hexagonal lattice of the overlayer, the next-neighbor Ti distance is 344 pm and this structure is rotated by ±15° with respect to Ru(0001).

Upon annealing in UHV to 1250 K, the material rearranges in a different periodic structure. The STM image of **Figure 2**a reveals a homogeneous dense packing of the atoms at the surface. Minor height variations occur that result in stripe-like trenches as emphasized by the white lines in Figure 2a. The FT of (a) shown as an inset unravels a quadratic structure of this phase. The close-up STM image in Figure 2b reveals the formation of a five vertex structure on the atomic scale: Each protrusion is surrounded by five next neighbors at equal distance. The repeating motif of this structure is an arrangement of four triangles and two squares as marked in black in Figure 2b. The resulting unit cell containing four Ti atoms is marked in blue. The stripe-like height modulation seen in the STM of Figure 2a is linked to the unit cell dimensions. The stripes occur under 45° and have a spacing corresponding to the unit cell diagonal. This structure is called $\sigma$-phase in the context of periodic approximant structures related to quasicrystals as described by Förster et al.[18] Previously, a $\sigma$-phase structure has been reported in the $BaTiO_3$/Pt(111) system.[19–21] In a detailed analysis involving STM, LEED, surface X-ray diffraction (SXRD), and density functional theory calculations, the tiling has been identified as the Ti sublattice of the 2D reduced $BaTiO_3$ layer. The STM data presented in Figure 2a,b has been recorded at a high negative bias voltage of −2.6 V, which shows that the Ti atoms dominated the STM contrast even far from the Fermi level.

Figure 2c–e show two LEED pattern as well as a simulation of the measured LEED data of the $\sigma$-phase structure derived from $BaTiO_3$ on Ru(0001). At low kinetic energies (Figure 2c), the pattern of the $\sigma$-phase on Ru(0001) is characterized by a 12-fold arrangement of triangular sets of spots. This apparent 12-fold symmetry results from a coexistence of three rotational domains of this structure at the Ru(0001) surface as indicated in Figure 2e. In the intensity distribution of higher-order spots at 2.0 $Å^{-1}$ (marked by the circle in Figure 2e), a clear reduction of the 12-fold to a 6-fold symmetry is seen. In alternating sequence every 30° three spots are either almost completely overlapping, or well-separated from each other. The pattern is simulated with a commensurate superstructure as it was the case for the hexagonal structure discussed previously. The $\sigma$-phase unit cell is described by a $\begin{pmatrix} 4 & -1.5 \\ 4 & 5.5 \end{pmatrix}$ superstructure matrix with respect to Ru(0001). This unit cell is almost quadratic. It has equal unit vectors with a length of 1.33 nm that incline to an angle of 90.6°. The unit cell is rotated by ±15.3° out of the high symmetry directions of the substrate. The coincidence cell of the $\sigma$-phase with the Ru(0001) substrate is given by $\begin{pmatrix} 8 & -4 \\ 7 & 0 \end{pmatrix}$. This is a $(\sqrt{2} \times \sqrt{2})R45°$ superstructure with respect to the $\sigma$-phase. The periodicity of systematic height variation of the $\sigma$-phase seen in STM (Figure 2a) is determined by the coincidence cell unit vector.

The reported sequence of structures is robust upon cycles of oxygen and UHV annealing. For $BaTiO_3$/Pt(111), it has been demonstrated that these cycles corresponds to a reversible transformation of the oxide material from fully oxidized periodic islands to reduced 2D wetting layers.[16] This is also the case for $BaTiO_3$ on Ru(0001). Upon oxygen annealing, the 2D wetting layer disappears and 3D oxide islands are formed. During subsequent UHV annealing, the hexagonal superstructure is observed in the lower temperature regime, and with increasing temperature, the $\sigma$-phase develops. This procedure has been repeated multiple times without a noticeable change in the Ba:Ti composition on Ru(0001).

The hexagonal phase also develops in ultrathin reduced $SrTiO_3$ on Pt(111). There, a monoclinic approximant to the OQC has been observed for stoichiometric monolayers, which is characterized by a unit cell formed from 36 tiles out of the OQC tiling.[15] Upon increasing the Ti content by roughly 15%, the hexagonal superstructure occurs. **Figure 3**a shows a


© 2020 The Authors. Published by WILEY-VCH Verlag GmbH & Co. KGaA, Weinheim

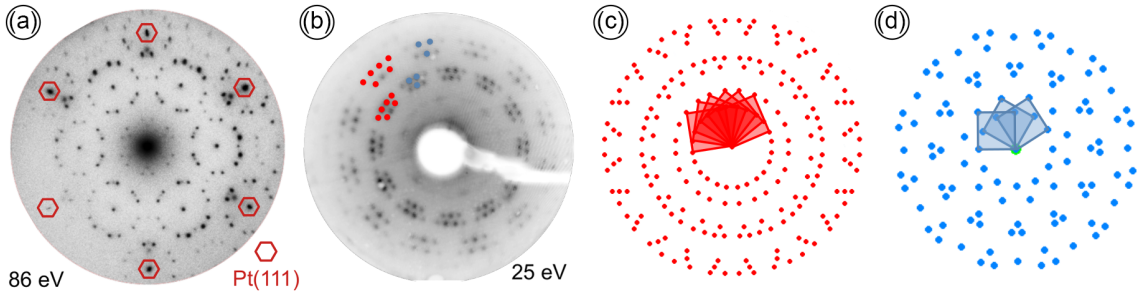


**Figure 3.** a) SPALEED image recorded for a 2D reduced $SrTiO_3$ layer on Pt(111) at an energy of 86 eV. It shows a similar hexagonal superstructure as seen in Figure 1d. b) LEED image with a superposition of two different $\sigma$-phase orientations derived from $BaTiO_3$ on Pt(111) taken at 25 eV. In red the spots of the previously reported 8° rotated $\sigma$-phase approximant are marked. The spots in blue correspond to a 15.1° rotated $\sigma$-phase. c,d) LEED simulation of the 8° and the 15.1° rotated $\sigma$ phase, respectively. The solid red and blue squares indicate the different domains that contribute in LEED.

spot-profile analysis low-energy electron (SPALEED) diffraction pattern taken upon UHV annealing to 1100 K. The structure is described by a $\begin{pmatrix} 5 & 1 \\ 4 & 5 \end{pmatrix}$ superstructure matrix, which is identical with the one reported for this structure on Ru(0001). Due to a 2.6% increased substrate lattice constant when substituting Ru(0001) by Pt(111), the unit cell dimensions change by this value. This results in a lattice parameter of 1.27 nm for the superstructure and changes the interatomic spacing for the primitive hexagonal lattice of neighboring Ti atoms from 344 to 353 pm.

The $\sigma$-phase superstructure reported previously for $BaTiO_3$ on Ru(0001) is also formed as additional phase in the $BaTiO_3$/Pt(111) system. Figure 3b shows a LEED pattern recorded upon annealing a 0.3 nm thin $BaTiO_3$ layer to 1200 K in UHV. In this particular preparation, the well-established $\sigma$-phase on Pt(111) which is rotated by ±8° against the Pt(111) substrate has formed[19] (marked in red in Figure 3b). However, the LEED pattern shows additional spots, which originate from a ±15° rotated $\sigma$-phase as discussed previously for $BaTiO_3$ on Ru(0001). The spots of both rotations of the $\sigma$-phase on Pt(111) are aligned on circles in the LEED pattern of Figure 3b, indicating a similar lattice constant. The simulated LEED pattern of both orientations are shown in Figure 3c,d. The unit cell of this new rotational variant of the $\sigma$-phase on Pt(111) is given by $\begin{pmatrix} 3.8 & -1.4 \\ 3.8 & 5.2 \end{pmatrix}$. It is rotated 15.1° against the substrate. Its unit vectors have a common length of 1.29 nm and incline to an angle of 90.2°. This unit vector length is identical to the short unit cell vector of the 8° rotated $\sigma$-phase.[19] The coincidence cell of the 15° rotated $\sigma$-phase is described by $\begin{pmatrix} 19 & -7 \\ 19 & 26 \end{pmatrix}$ and contains a patch of 5 × 5 $\sigma$-phase units. The difference in the number of spots for the different rotations results from a coincidence of the mirror domain spots. This is illustrated by the solid squares representing the different domains in the calculated pattern of Figure 3c,d.

## 3. Discussion

**Table 1** summarizes the structural parameters of the 2D wetting layer structures derived above for $BaTiO_3$ on Ru(0001), $BaTiO_3$ on Pt(111), and $SrTiO_3$ on Pt(111).[15,19]

The two superstructures that are formed from $BaTiO_3$ on Ru(0001) show strong variations in the spacing of Ti atoms. For the hexagonal phase, a Ti–Ti distance of 344 pm has been determined. In contrast, upon annealing to higher temperatures, a twice as large spacing of 688 pm develops. The smaller value is close to the lattice spacing in pure $TiO_x$ monolayer structures on metal surfaces like Pt,[23–25] Mo,[26,27] Cu,[28] Ni,[29] Au,[30,31] and Pd.[32] However, two facts clarify that the hexagonal superstructure is formed indeed by the ternary oxide and not from a binary $TiO_x$. First, the $\sigma$-phase structure is known to form at a 1:1 ratio of the Ba and Ti.[19] Consequently, from the ability to reversibly

**Table 1.** Structural parameters of periodic superstructures observed for $BaTiO_3$/Ru(0001), $BaTiO_3$/Pt(111), and $SrTiO_3$/Pt(111): the average distance of neighboring Ti atoms, the superstructure matrices for the coincidence cells, the number of primitive unit cells of the $\sigma$-phase per coincidence cell and the superstructure matrices of the primitive cells with respect to Pt(111)/Ru(0001), and the orientation of Ti pairs with respect to the given substrate.

| | Hexagonal phase | $\sigma$-phase | | | | |
|---|---|---|---|---|---|---|
| | Ti–Ti distance | Coincidence cell | $\sigma$-phase units | | Ti–Ti orientation | Ti–Ti distance [pm] |
| $BaTiO_3$/Ru(0001) | 344 pm | $\begin{pmatrix} 8 & -4 \\ 7 & 0 \end{pmatrix}$ | $(\sqrt{2} \times \sqrt{2})R45°$ | $\begin{pmatrix} 4 & -1.5 \\ 4 & 5.5 \end{pmatrix}$ | \|\| to substrate | 688 |
| $BaTiO_3$/Pt(111) | – | $\begin{pmatrix} 19 & -7 \\ 19 & 26 \end{pmatrix}$ | 5 × 5 | $\begin{pmatrix} 3.8 & -1.4 \\ 3.8 & 5.2 \end{pmatrix}$ | \|\| to substrate | 668 |
| $BaTiO_3$/Pt(111)[19] | – | $\begin{pmatrix} 27 & 10 \\ 3 & 20 \end{pmatrix}$ | 5 × 4 | $\begin{pmatrix} 27/5 & 2 \\ 3/4 & 5 \end{pmatrix}$ | 7° versus substrate | 673 |
| $SrTiO_3$/Pt(111) | 353 pm | 36 tiles approximant[15] | | | \|\| to substrate | 672 |


© 2020 The Authors. Published by WILEY-VCH Verlag GmbH & Co. KGaA, Weinheim

change between the two structures by oxidation and subsequent UHV annealing, an equal metal composition must apply to the hexagonal phase. Second, the structure was not reported earlier, although ultrathin films of $TiO_2$ have been a topic of research for decades. From the literature, it is known that $TiO_2$ on Ru(0001) forms a $(5\sqrt{3} \times 5\sqrt{3})R30^\circ$ superstructure for 0.68 ML Ti deposited in $O_2$ atmosphere[33] or a $(6\sqrt{3} \times 6\sqrt{3})$ superstructure after flash annealing 1 ML to 1000 K in $O_2$ atmosphere.[34] The atypical wide interatomic spacing in the $\sigma$-phase, which is, for example, much larger than the distance of Ti atoms in a hexagonal plane of $BaTiO_3$(111) of 566 pm, results from a planar arrangement of Ba, Ti, and O atoms in the 2D layer. In turn, the short distance as determined for the hexagonal superstructure points toward a vertical stacking of Ba and Ti atoms in the layer. To further support this structural model, complementary methods, e.g., SXRD or photoelectron diffraction, are needed.

Surprisingly, the Ti–Ti distance in the hexagonal phase of $SrTiO_3$ on Pt(111) of 353 pm is 2.6% larger as compared with that found for $BaTiO_3$ on Ru(0001). From the cation exchange in the wetting layer, a decrease in the wetting layer lattice parameter could have been expected, as the ionic radius of Sr is smaller as compared with that of Ba. A change in the opposite direction indicates a large flexibility in the wetting layer structure and emphasizes a stronger interaction with the Ru(0001) substrate as compared with Pt(111).

A comparison of the structural parameters of the $\sigma$-phase on different substrates in Table 1 pinpoints a significantly increased wetting-layer-substrate interaction for the Ru(0001) surface in comparison to Pt(111). The $\sigma$-phase on Ru(0001) realizes the smallest coincidence cell in this list. A patch of only twice the area of the $\sigma$-phase unit cell is needed to be commensurate with the substrate. To achieve this match, the Ti–Ti distance is significantly expanded as compared with the $\sigma$-phase formed by $BaTiO_3$ on Pt(111). It is more than 2% larger on Ru(0001) despite a decrease in the substrate lattice constant. In addition to the small coincidence cell, also the parallel alignment of the Ti–Ti pairs to the high-symmetry substrate directions indicates a strong wetting-layer-substrate interaction. **Figure 4** shows the $\sigma$-phase alignment for the coincidence cells of the $\sigma$-phase on Ru(0001), the 8° rotated $\sigma$-phase on Pt(111), and the 36 tiles approximant of $SrTiO_3$ on Pt(111). The latter is included in the comparison of Table 1 and in Figure 4, as its unit cell contains a large patch of the $\sigma$-phase as marked by the enlightened area in Figure 4. In case of $SrTiO_3$/Pt(111), the Ti–Ti distance is comparable to the $\sigma$-phase observed on Pt(111). This fact shows, that the cation exchange from Ba to Sr does not alter the wetting layer structure and does not affect the wetting-layer-substrate interaction. An additional manifestation of the comparably weaker interaction of the wetting layer with the Pt(111) surface are the large coincidence cells of the $\sigma$-phase. Figure 4 shows the example for the 8° rotated $\sigma$-phase for which a patch of $4 \times 5$ $\sigma$-phase is needed to achieve a substrate registry. In case of the 15° rotated $\sigma$-phase on Pt(111), even a mesh of $5 \times 5$ units is needed.

Although ultrathin films of $BaTiO_3$ on Ru(0001) have been prepared in slightly varying compositions and by different deposition techniques (rf magnetron sputtering and MBE), no other structures have been observed in this system, especially no OQC is formed. This is surprising, as the diffraction pattern of the $\sigma$-phase under 15° rotation against the substrate resembles a very good approximation to the dodecagonal structure of OQCs. In case of a transformation into a dodecagonal structure, the triangular sets of spots in the LEED pattern would collapse into a single spot in the centers of the triangles. The presented facts emphasize that the strong epitaxial stabilization of the $\sigma$-phase on Ru(0001) suppresses an OQC formation of $BaTiO_3$ on Ru(0001).

## 4. Conclusion

2D structures in reduced wetting layers of $BaTiO_3$ on Ru(0001) and Pt(111) and $SrTiO_3$ on Pt(111) are reported. Upon UHV

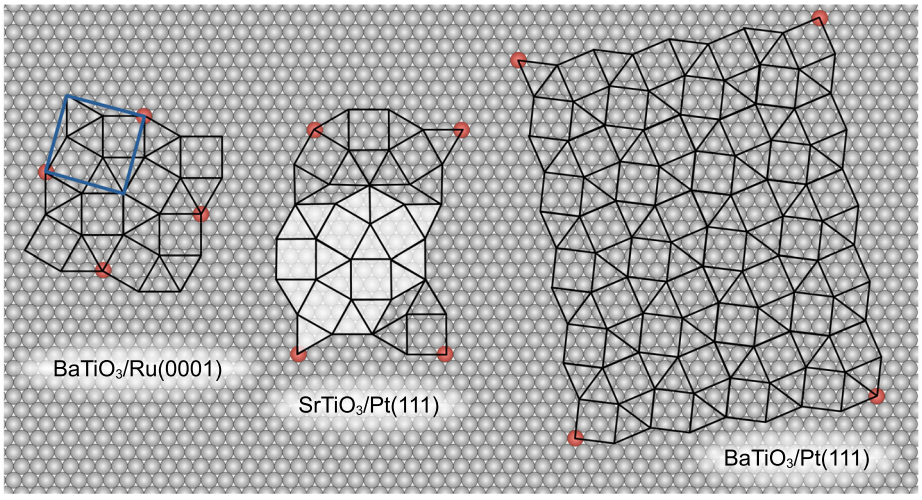


**Figure 4.** Wetting layer structures observed for ternary oxides on Ru(0001) and Pt(111). The meshes drawn in black mimic the sublattices of Ti atoms in these structures. The red balls mark the size of the coincidence cells. The blue rectangle marks a primitive unit cell of the $\sigma$-phase of $BaTiO_3$ on Ru(0001). The enlightened area in the unit cell of $SrTiO_3$/Pt(111) marks a tiling patch similar to the $\sigma$-phase. The large patch on the right depicts the coincidence cell of the 8° rotated $\sigma$-phase of $BaTiO_3$ on Pt(111).


© 2020 The Authors. Published by WILEY-VCH Verlag GmbH & Co. KGaA, Weinheim

annealing at 1100 K, a hexagonal superstructure with a Ti–Ti distance of 344 pm is observed in $BaTiO_3$/Ru(0001). A similar superstructure develops in $SrTiO_3$/Pt(111) for which the Ti–Ti distance is increased by 2.9%. For $BaTiO_3$/Ru(0001), a transformation into a triangle-square tiling with a Ti–Ti of distance 688 pm is observed upon annealing at 1250 K in UHV. This triangle-square tiling is known as $\sigma$-phase approximant to the OQC discovered in $BaTiO_3$/Pt(111).[1,19] A 2.2 % expansion of the Ti–Ti distance and a small area $\begin{pmatrix} 8 & -4 \\ 7 & 0 \end{pmatrix}$ coincidence cell for the $\sigma$-phase of $BaTiO_3$/Ru(0001) emphasize a stronger interaction of the reduced oxide to Ru(0001) as compared to Pt(111). The epitaxial stabilization of the $\sigma$-phase on Ru(0001) seems to suppress the formation of a dodecagonal structure in the $BaTiO_3$/Ru(0001) system.

## 5. Experimental Section

The experiments were performed in UHV systems operating at a base pressure of $10^{-10}$ mbar. Pt(111) substrates (Mateck, Germany) were cleaned by repeating cycles of $Ar^+$ ion sputtering and annealing as described in ref. [1]. The Ru(0001) substrate was also cleaned by cycles of $Ar^+$ ion sputtering and annealing. Each annealing step contained multiple cycles of the following annealing procedure: 1) annealing to 670 and 870 K in $2 \times 10^{-8}$ mbar $O_2$ for 2 min, respectively. 2) Cooling down to RT for 3 min in UHV. 3) Flash to 1470 K in $6 \times 10^{-9}$ mbar $O_2$ for 1 min. For temperature measurements, a pyrometer (Cyclops 52, Minolta, $\lambda = 520$ nm) was used at $\varepsilon = 0.1$ optimized to the Pt and Ru substrates. Ultrathin films of $SrTiO_3$ and $BaTiO_3$ were deposited by MBE from a Nb-doped (0.05%) $SrTiO_3$ single crystal and a stoichiometric $BaTiO_3$ ceramic as described in detail in ref. [15,35].

## Acknowledgements

The authors thank Karl-Michael Schindler for fruitful discussions. The authors gratefully acknowledge technical support by Ralf Kulla. Financial support was provided from the Deutsche Forschungsgemeinschaft (DFG) through the collaborative research center SFB 762 (Functionality of Oxide Interfaces, project A3).

## Conflict of Interest

The authors declare no conflict of interest.

## Keywords

low-energy electron diffraction, oxide quasicrystals, scanning tunneling microscopy, σ-phase approximant

Received: October 15, 2019
Revised: December 20, 2019
Published online: January 22, 2020

[1] S. Förster, K. Meinel, R. Hammer, M. Trautmann, W. Widdra, *Nature* **2013**, *502*, 215.
[2] K. Urban, N. Moser, H. Kronmüller, *Phys. Status Solidi A* **1985**, *91*, 411.
[3] Z. Zhang, K. Urban, *Scr. Metall. Mater.* **1989**, *23*, 1663.
[4] Y. Zhuang, Z. Zhang, D. B. Williams, *J. Non-Cryst. Solids* **1993**, *153*, 119.
[5] V. Fournée, P. A. Thiel, J. Phys, *D: Appl. Phys.* **2005**, *38*, 83.
[6] H.-R. Sharma, M. Shimoda, A. P. Tsai, *Adv. Phys.* **2007**, *56*, 403.
[7] V. Fournée, J. Ledieu, M. Shimoda, M. Kraj, H.-R. Sharma, R. McGrath, *Isr. J. Chem.* **2011**, *51*, 1314.
[8] F. C. Frank, J. H. van der Merwe, *Proc. R. Soc. Lond. A* **1949**, *198*, 205.
[9] A. Hoshino, S. Isoda, H. Kurata, T. Kobayashi, *J. Appl. Phys.* **1994**, *76*, 4113.
[10] G. Friedel, *Lecon De Cristallographie* Berger Levrault, Paris, **1926**.
[11] M. L. Kronberg, F. H. Wilson, *Trans. AIME* **1949**, *185*, 501.
[12] N. H. Fletcher, *J. Appl. Phys.* **1964**, *35*, 234.
[13] E. J. Widjaja, L. D. Marks, *Philos. Mag. Lett.* **2003**, *83*, 47.
[14] K. J. Franke, P. Gille, K.-H. Rieder, W. Theis, *Phys. Rev. Lett.* **2007**, *99*, 036103.
[15] S. Schenk, S. Förster, K. Meinel, R. Hammer, B. Leibundgut, M. Paleschke, J. Pantzer, C. Dresler, F. O. Schumann, W. Widdra, *J. Phys.: Condens. Matter* **2017**, *29*, 134002.
[16] S. Förster, J. I. Flege, E. M. Zollner, F. O. Schumann, R. Hammer, A. Bayat, K.-M. Schindler, J. Falta, W. Widdra, *Ann. Phys. (Berlin)* **2017**, *529*, 1600250.
[17] S. Schenk, E. M. Zollner, O. Krahn, B. Schreck, R. Hammer, S. Förster, W. Widdra, *Acta Cryst.* **2019**, *A75*, 307.
[18] S. Förster, S. Schenk, E. M. Zollner, O. Krahn, C.-T. Chiang, F. O. Schumann, A. Bayat, K.-M. Schindler, M. Trautmann, R. Hammer, K. Meinel, W. A. Adeagbo, W. Hergert, J. I. Flege, J. Falta, M. Ellguth, C. Tusche, M. DeBoissieu, M. Muntwiler, T. Greber, W. Widdra, *Phys. Status Solidi B* **2020**, *257*, 1900624. (in this issue)
[19] S. Förster, M. Trautmann, S. Roy, W. A. Adeagbo, E. M. Zollner, R. Hammer, F. O. Schumann, K. Meinel, S. K. Nayak, K. Mohseni, W. Hergert, H. L. Meyerheim, W. Widdra, *Phys. Rev. Lett.* **2016**, *117*, 095501.
[20] K. Mohseni Roy, S. Förster, M. Trautmann, F. Schumann, E. Zollner, H. Meyerheim, W. Widdra, Z. Kristallogr, *Z. Kristallogr. Cryst. Mater.* **2016**, *231*, 749.
[21] K. Mohseni, H. L. Meyerheim, *Phys. Status Solidi B* **2020**, *257*, 1900605. (in this issue)
[22] C.-T. Chiang, M. Ellguth, F. O. Schumann, C. Tusche, R. Kraska, S. Förster, W. Widdra, *Phys. Rev. B* **2019**, *100*, 125149.
[23] A. B. Boffa, H. C. Galloway, P. W. Jacobs, J. J. Benitez, J. D. Batteas, M. Salmeron, A. T. Bell, G. A. Somorjai, *Surf. Sci.* **1995**, *326*, 80.
[24] F. Sedona, G. A. Rizzi, S. Agnoli, F. X. Llabres i Xamena, A. Papageorgiou, D. Ostermann, M. Sambi, P. Finetti, K. Schierbaum, G. Granozzi, *J. Phys. Chem.* **2005**, *109*, 24411.
[25] G. Barcaro, E. Cavaliere, L. Artiglia, L. Sementa, L. Gavioli, G. Granozzi, A. Fortunelli, *J. Phys. Chem. C* **2012**, *116*, 13302.
[26] Q. Guo, W. S. Oh, D. W. Goodman, *Surf. Sci.* **1999**, *437*, 49.
[27] W. S. Oh, C. Xu, D. Y. Kim, D. W. Goodman, *J. Vac. Sci. Technol. A* **1997**, *15*, 1710.
[28] T. Maeda, Y. Kobayashi, K. Kishi, *Surf. Sci.* **1999**, *436*, 249.
[29] T. V. Ashworth, G. Thornton, *Thin Solid Films* **2001**, *400*, 43.
[30] Z. Song, J. Hrbek, R. Osgood, *Nano Lett.* **2005**, *5*, 1327.
[31] C. Wu, M. S. J. Marshall, M. R. J. Castell, *J. Phys. Chem. C* **2011**, *115*, 8643.
[32] R. A. Bennett, C. L. Pang, N. Perkins, R. D. Smith, P. Morrall, R. I. Kvon, M. Bowker, *J. Phys. Chem. B* **2002**, *106*, 4688.
[33] J. P. S. Badyal, A. J. Gellman, R. W. Judd, R. M. Lambert, *Catal. Lett.* **1988**, *1*, 41.
[34] A. Männig, Z. Zhao, D. Rosenthal, K. Christmann, H. Hoster, H. Rauscher, R. J. Behm, *Surf. Sci.* **2005**, *576*, 29.
[35] E. M. Zollner, S. Schenk, M. Setvin, S. Förster, *Phys. Status Solidi B* **2020**, *257*, 1900620. (in this issue)


© 2020 The Authors. Published by WILEY-VCH Verlag GmbH & Co. KGaA, Weinheim